ADVANCED PHOTONICS RESEARCH
Open Access
www.adpr-journal.com

Below 1% Reflectance for Black GaAs Surface Prepared by Facile Two-Step Wet Chemical Treatment: Hydrogen Peroxide and Water

Zahra Jahanshah Rad, Johanna Laaksonen, Valtteri Alitupa, Mikko Miettinen, Kari Iltanen, Juha-Pekka Lehtiö, Sari Granroth, Ilari Angervo, Marko Punkkinen, Risto Punkkinen, Mikhail Kuzmin, Ermei Mäkilä, Pekka Laukkanen,* Petriina Paturi, Kalevi Kokko, Sami Vuori, Mika Lastusaari, Harishchandra Singh, Marko Huttula, Manvedra Narayan Singh, Antti Tukiainen, Heidi Tuorila, Helmer Piirilä, Jukka Viheriälä, Mircea Guina, Jekaterina Kozlova, Mihkel Rähn, and Aile Tamm*

To increase performance of many photonic devices (e.g., solar cell, light emitting diode (LED), photodetector), it is essential to decrease light reflection at device interfaces. Sustainable and scalable methods have been intensively developed for manufacturing nanostructured antireflection coatings at device surfaces to reduce the reflection-induced losses in them. In this work, a novel wet chemical method is demonstrated to prepare black nanostructured GaAs surfaces in scalable manner. This facile method includes two steps: immersion of GaAs in hot H_2O_2 solution followed by immersion in hot H_2O both at around 80 °C. Microscopy, spectroscopy, and diffraction measurements reveal that the H_2O_2 immersion increases a surface porosity at GaAs while the hot-water treatment causes the formation of GaOOH nanocrystals. Reflectivity at the resulting black GaAs surface is decreased even below 1% in a broadband. Photoluminescence intensity measurements are used to study whether the presented top-to-down method increases harmful non-radiative recombination, as compared to the initial GaAs surface. Integration of the found black-GaAs method with device manufacturing is presented by means of planar metal–GaAs–metal photodetectors, of which external quantum efficiency increases due to the method.

1. Introduction

Methods to manufacture nanostructures at semiconductor surfaces have attracted great interest in various disciplines, including photonics where the nanostructures for instance enable to reduce the light reflection–induced losses in devices.[1–15] In solar cells and photodetectors, nanostructured surfaces act as the antireflection coating to guide the light into semiconductors, while in LEDs, the surface nanostructures help to extract the light out from the solid efficiently. These engineered surfaces include for instance metal-assisted chemical etched nanostructures,[1,3,5,11,13] nanoneedles,[2] metal-oxide nanorods,[4,7] plasma etched nanograss,[6] and reactive-ion-etched nanocones[8,15] which are inspired by the moth-eye principles to suppress the reflection in a broad wavelength band. Toward large-scale use of a surface engineering method, it is beneficial that the method is facile and sustainable concerning the consumption of chemicals and energy.[16–19] Therefore, the development of manufacturing

Z. J. Rad, J. Laaksonen, V. Alitupa, M. Miettinen, K. Iltanen, J.-P. Lehtiö, S. Granroth, I. Angervo, M. Punkkinen, R. Punkkinen, M. Kuzmin, E. Mäkilä, P. Laukkanen, P. Paturi, K. Kokko
Department of Physics and Astronomy
University of Turku
FI-20014 Turku, Finland
E-mail: zahra.s.jahanshahrad@utu.fi; pekka.laukkanen@utu.fi

The ORCID identification number(s) for the author(s) of this article can be found under https://doi.org/10.1002/adpr.202400200.

© 2025 The Author(s). Advanced Photonics Research published by Wiley-VCH GmbH. This is an open access article under the terms of the Creative Commons Attribution License, which permits use, distribution and reproduction in any medium, provided the original work is properly cited.

DOI: 10.1002/adpr.202400200

S. Vuori, M. Lastusaari
Department of Chemistry
University of Turku
FI-20014 Turku, Finland

H. Singh, M. Huttula
Nano and Molecular Systems Research Unit
University of Oulu
FI-90014 Oulu, Finland

M. N. Singh
Synchrotrons Utilization Section
Raja Ramanna Centre for Advanced Technology
Indore 452013, India

protocols which enable for example to decrease the amount of lithography steps and toxic chemicals is important for advancing the field. Here, we report a novel method to prepare a black GaAs surface with the reflectivity even lower than 1% in 500–886 nm wavelength region. This method is surprisingly facile because it requires only an immersion of GaAs crystals in a hot H_2O_2 solution followed by an immersion in hot H_2O.

During the last 50 years,[20,21] GaAs crystals have become the established material of semiconductor industry. GaAs is used particularly in the light-emitting components and infrared sensors, in the devices where silicon performance is not high enough. Furthermore, the 850 nm laser and photodiode systems, based on GaAs, provide an emergent optical interconnection in the data storage and processing centers,[22–24] whereas high-efficiency and durable GaAs solar cells and photodiodes are increasingly employed in aerospace and power-by-light applications and also as local power sources via GaAs thin-film solutions.[25–31] Moreover, GaAs is also a potential electrode material for photoelectrochemical cells in hydrogen production.[32,33] Even the currently used GaAs-based devices suffer from different losses (e.g., reflection and nonradiative recombination ones) which decrease performance and manufacturing yield of the devices. One reason for the losses is surface areas of GaAs crystals which typically react with surrounding conditions, leading to changes in the GaAs surface properties.

This article is organized as follows: preparation of a black GaAs surface and its reflectivity properties are presented first. The hot-water immersion is a key step in the method according to our results, and therefore we have also studied properties of merely hot-water-treated GaAs surfaces. Because non-radiative recombination is readily increased at processed GaAs surfaces, in general, due to an increased density of point defects, we have used a photoluminescence (PL) intensity comparison to understand effects of the presented top-to-down method on defect formation. Finally, we show a potential approach to incorporate the black GaAs method into manufacturing devices by showing results for GaAs-based metal–semiconductor–metal (MSM) photodetectors.

2. Results and Discussion

2.1. Black GaAs Surface Characterization

Figure 1 presents a photo from a black GaAs surface and the reflectance spectra after different combinations of the hot hydrogen peroxide (H_2O_2) and subsequent hot-water (H_2O) immersion. Reflectance was measured by two different instruments (Section 4, Experimental Section). Our tests show that the lowest reflectance (<1%) is obtained when a bulk GaAs crystal is first kept in the hot H_2O_2 (80 °C) solution for 240 min and then in hot H_2O (80 °C) for 240 min, as shown in Figure 1a, where horizontal blue dot lines mark the levels of 1% and 2% reflectivities. The reflectance in Figure 1a is the specular one measured perpendicular to the surface (Section 4, Experimental Section). It is worth noting that an optimized combination of the hot H_2O_2 immersion followed by the hot H_2O one is expected to depend on a GaAs layer thickness and an integration stage with device manufacturing for instance.

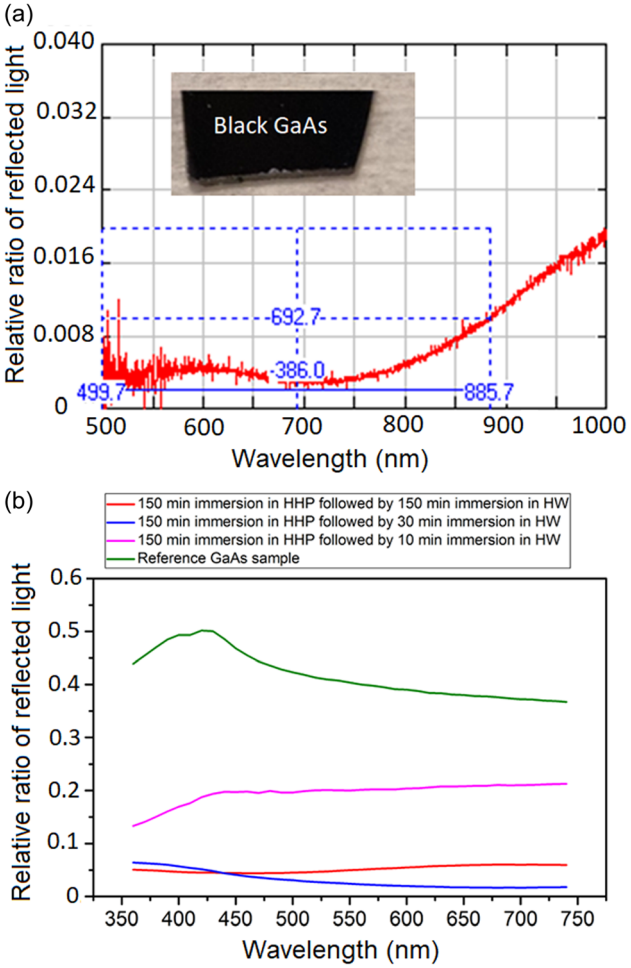

Figure 1. Reflectivity of black GaAs surfaces measured with two different setups. a) Specular reflectivity measured from a black GaAs surface prepared at 80 °C with 240 min hydrogen peroxide plus 240 min hot-water immersions. Inset shows a photo from black GaAs. b) Lambertian (diffused) reflectivity curves, in relation to GaAs reference sample, for different hot-water (HW) immersion times done after 150 min hot-hydrogen peroxide (HHP) immersion at 80 °C.

In Figure 1b, a separate series of treatments, where the H_2O_2 (80 °C) immersion time is fixed 150 min and the H_2O (80 °C) immersion time varies, is compared to the reflectance of native-oxide-covered GaAs. The measurements in Figure 1b are diffused (i.e., Lambertian) type, showing that the GaAs reflectance decreases even to 1/10 or less, as compared to the GaAs reference without any treatment, at the studied wavelength range of 360–740 nm. Because the 30 min H_2O immersion provides smaller reflection than the 150 min H_2O immersion at

A. Tukiainen, H. Tuorila, H. Piirilä, J. Viheriälä, M. Guina
Optoelectronics Research Centre
Tampere University
FI-33720 Tampere, Finland

J. Kozlova, M. Rähn, A. Tamm
Institute of Physics
University of Tartu
50411 Tartu, Estonia

© 2025 The Author(s). Advanced Photonics Research published by Wiley-VCH GmbH

26999293, 0, Downloaded from https://advanced.onlinelibrary.wiley.com/doi/10.1002/adpr.202400200 by University of Turku, Wiley Online Library on [11/08/2025]. See the Terms and Conditions (https://onlinelibrary.wiley.com/terms-and-conditions) on Wiley Online Library for rules of use; OA articles are governed by the applicable Creative Commons License

450–740 nm in Figure 1b, the effect does not have a simple inversely proportional dependence on the immersion times. Future studies can clarify this issue and a possible interplay between different treatment parameters. Each solution immersion alone, H_2O_2 or H_2O decreases also the reflectance, as shown later. However, only the combination of the H_2O_2 and subsequent H_2O immersions provides the lowest reflectance and a visually black GaAs surface (Figure 1), according to our observations.

Figure 2 shows scanning electron microscopy (SEM) and energy-dispersive X-ray (EDX) spectroscopy results after the H_2O_2 immersion and after the combination H_2O_2 plus H_2O. The subsequent H_2O immersion significantly decreases the As/Ga ratio and increases the amount of oxygen incorporated into GaAs. X-ray photoelectron spectroscopy (XPS) measurements also indicate that the surface does not contain anymore the substrate-like Ga—As bonding after the hot-water step (Figure S1, Supporting Information). The XPS results show that the amount of Ga oxide increases also in the H_2O_2 immersion, as compared to the native-oxide-covered surface, while the amount of As oxide does not change significantly. After the combination of H_2O_2 (150 min) + H_2O (10 min), the As 3d emission from the pure GaAs substrate decreases significantly (Figure S1, Supporting Information).

Furthermore, the SEM images (Figure 2) indicate that a basic porous structure, induced in hot H_2O_2, remains on large scale after the hot-water treatment. However, an additional nanostructure forms at GaAs in the hot H_2O solution according to the SEM images (Figure 2). To study further the structure of a black GaAs surface, scanning transmission electron microscopy (STEM) of the cross-sectional sample was carried out (**Figure 3**). The STEM images show that a thickness of the GaAs surface part, affected by the wet chemical treatments (i.e., H_2O_2, 80 °C, 150 min + H_2O, 80 °C, 30 min), is locally larger than 100 nm. Figure 3b indicates the formation of small crystals in the porous surface. Cross-sectional EDX mapping in Figure 3c–f shows that the black surface area is rich in oxygen, whereas the As signal in this close-to-surface region has decreased clearly. The oxygen-rich areas also show a high Ga signal, which supports the formation of a gallium oxide–rich layer in the surface region of GaAs. Furthermore, some surface areas in Figure 3c–f reveal a drop in the content of all mapped elements, indicating the formation of relatively deep pores, consistent with the earlier-described porosity. To get an understanding of the gallium oxide formation and to reveal a gallium oxide phase, we have investigated the influence of mere hot-water treatments on GaAs.

2.2. Effects of Mere H_2O Immersion

Figure 4 presents the SEM image for hot-water-induced nano- and microcrystals on GaAs. These samples were chemically pre-cleaned in HCl:IPA solution and then were immersed into hot water for 150 min. The water temperature was 80 °C. Spectroscopy maps indicate that Ga and O are dominant elements of the crystals at GaAs and that the substrate area between crystals consists of Ga, As, and O (Figure S2, Supporting Information). These results suggest that the crystals formed at

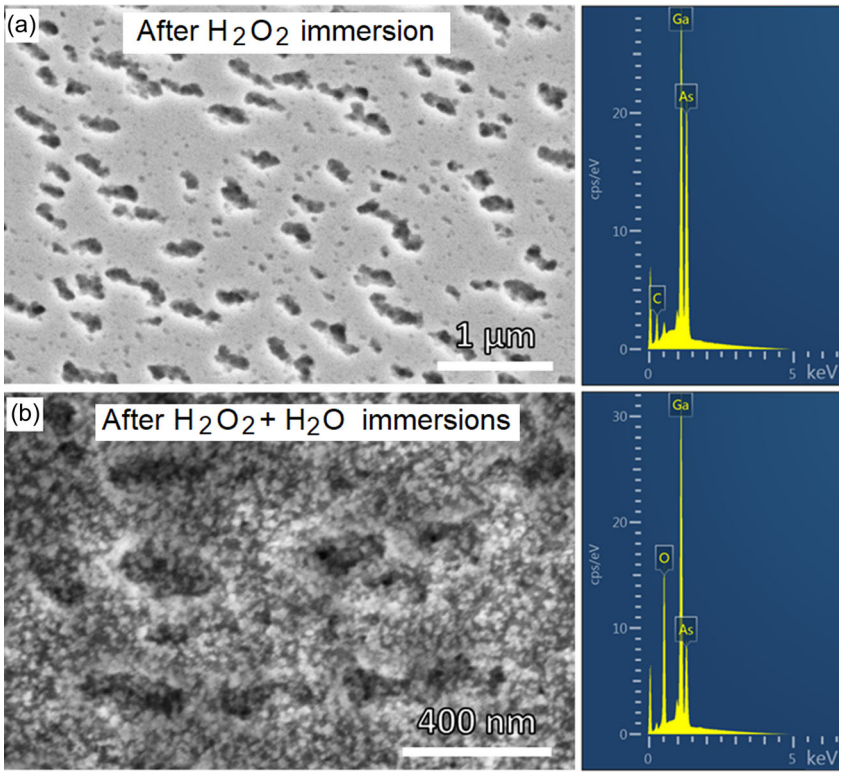

Figure 2. Scanning electron microscopy characterization of GaAs a) after H_2O_2 immersion (top) and b) after H_2O_2 + H_2O immersions (bottom). EDX results of the surface for each image are shown in the right panel.

© 2025 The Author(s). Advanced Photonics Research published by Wiley-VCH GmbH

26999293, 0, Downloaded from https://advanced.onlinelibrary.wiley.com/doi/10.1002/adpr.202400200 by University of Turku, Wiley Online Library on [11/08/2025]. See the Terms and Conditions (https://onlinelibrary.wiley.com/terms-and-conditions) on Wiley Online Library for rules of use; OA articles are governed by the applicable Creative Commons License

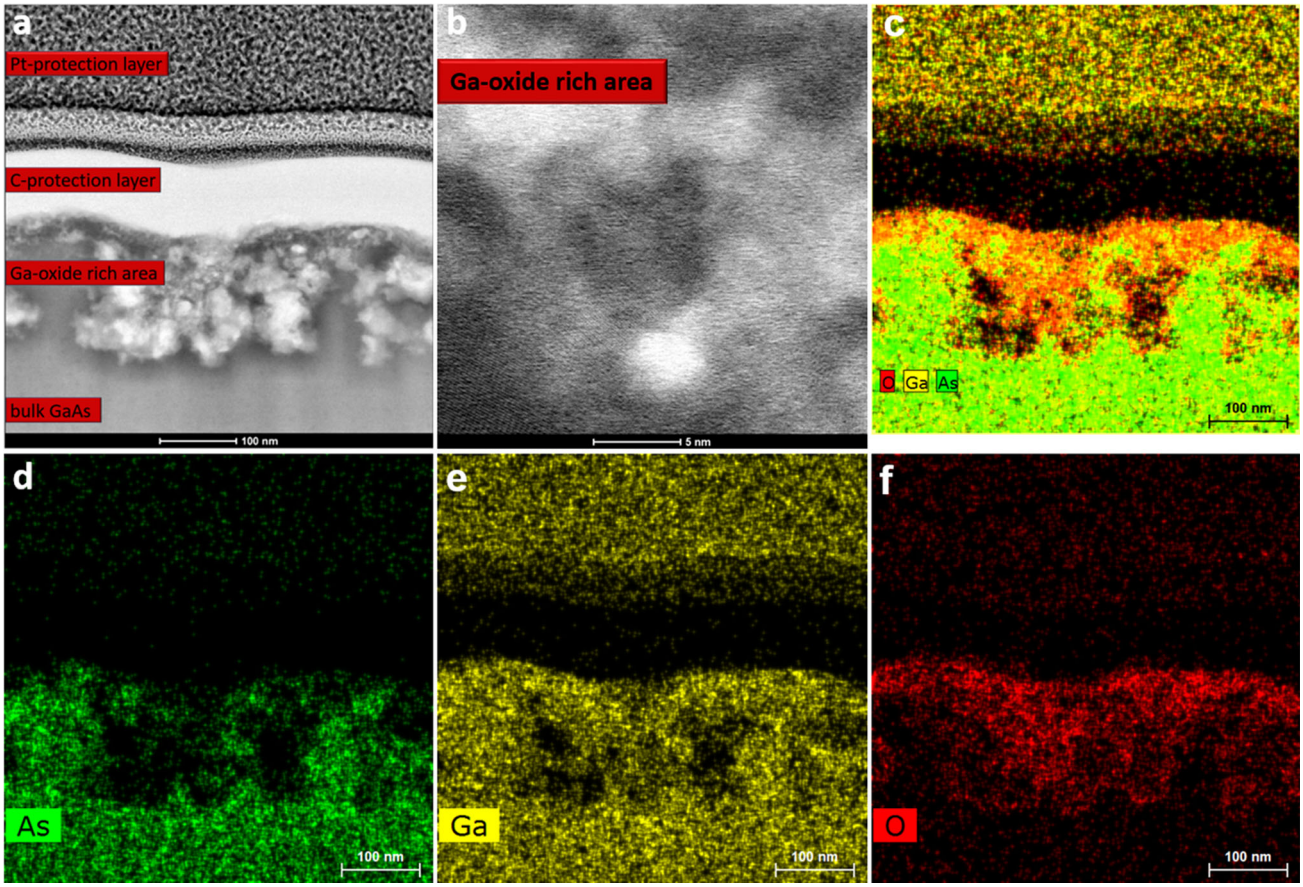

Figure 3. a,b) Cross-sectional bright-filed STEM images of the surface area of the GaAs after $H_2O_2 + H_2O$ immersion. c–f) STEM–EDX maps of As, Ga, and O in the region shown in (a). An increased Ga signal in the Pt-protection layer is due to the deposition of that layer by the Ga-ion beam.

GaAs consist of Ga_2O_3. Further characterization is still required to understand the crystal structure since it is not possible to detect hydrogen and crystal lattice using SEM. Therefore, grazing incidence synchrotron X-ray diffraction (GI-SXRD) measurements were performed. The diffraction results shown in Figure 4b reveal that the grown crystals are GaOOH. The results also suggest that the substrate surface orientation does not affect the growing phase, as the same GaOOH is observed at GaAs(111)-B and GaAs(100) substrates. The found GaOOH crystals indeed resemble the previously grown GaOOH crystals in microscopy images.[34–38] The presented hot-water approach in this work is, in fact, one of the most facile methods to grow GaOOH crystals. The Ga oxide materials have potential applications in different areas such as ultraviolet sensing and power electronics where devices need to tolerate harsh conditions.[39,40] The presented hot-water treatment of GaAs provides an interesting approach to making the hybrid materials combining III–V and Ga oxides.

To recapitulate, the results indicate that the nanocrystals, formed at the black GaAs surface after the second step of the H_2O immersion, contain GaOOH phase. The porous starting surface, prepared first by hot H_2O_2, appears to restrict a size of nanocrystals and hinders formation of the large microcrystals of GaOOH.

To get further support for the presence of hydrogen, some samples were post-heated in ultrahigh vacuum (UHV) because hydrogen readily diffuses in solids at elevated temperatures. The hot-water-modified samples were heated at 450 or 600 °C in a UHV chamber for 4 h. The laboratory source–based XRD and also GI-SXRD results in Figure S3 and S4 show a clear change in the peak positions, which indicates a start of the phase transition from GaOOH to Ga_2O_3 at 450–600 °C. It is worth noting that an SEM image after the 450 or 600 °C heating is very similar to that in Figure 4a before the post-heating.

To discuss the growth mechanism(s) of GaOOH crystals, different parameters were studied for the hot-water immersion. We clarified effects of a pre-cleaning method, hot-water immersion time, temperature, and amount of water on the growth. Figure S5a–c, Supporting Information, shows SEM results for GaAs substrates immersed in hot water for 15, 30, and 150 min, respectively, while keeping the water temperature constant at 80 °C. No growth was observed by SEM after the 5 min immersion, while small nucleation was seen after 15 min (Figure S5a, Supporting Information). After 30 min, the crystals are larger and their density is increased (Figure S5b, Supporting Information). After the 150 min immersion, the crystals are even larger with length of up to 7 μm and their density has increased further (Figure S5c, Supporting Information). Thus, we conclude

© 2025 The Author(s). Advanced Photonics Research published by Wiley-VCH GmbH

26999293, 0, Downloaded from https://advanced.onlinelibrary.wiley.com/doi/10.1002/adpr.202400200 by University of Turku, Wiley Online Library on [11/08/2025]. See the Terms and Conditions (https://onlinelibrary.wiley.com/terms-and-conditions) on Wiley Online Library for rules of use; OA articles are governed by the applicable Creative Commons License

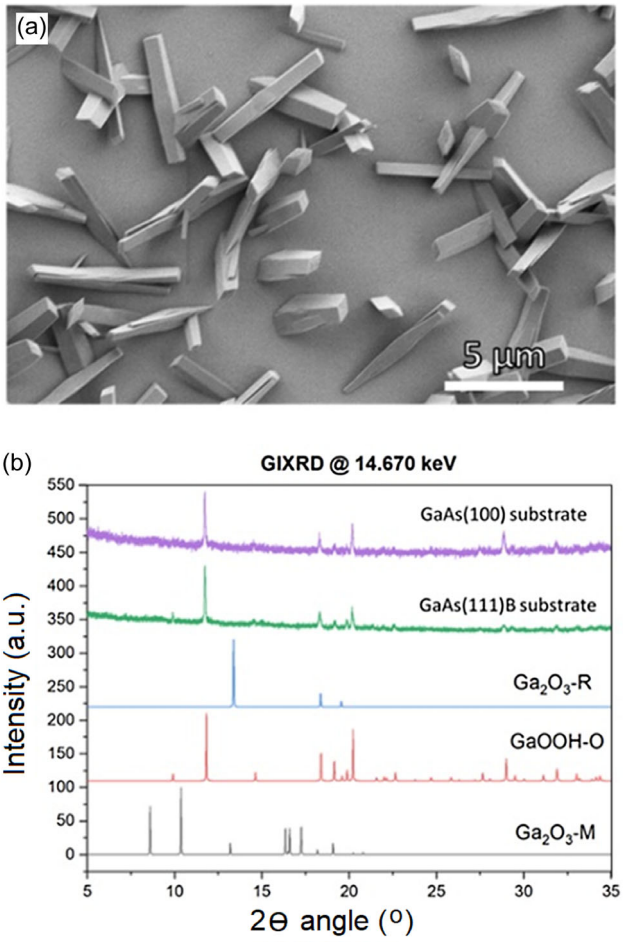

Figure 4. a) Scanning electron microscopy characterization of the hot-water-induced crystals on GaAs substrates at 80 °C. b) GI-SXRD of nanocrystals grown on GaAs(100) and GaAs(111)B substrates by immersing the substrates into hot water at 80 °C for 150 min. The results suggest formation of GaOOH phase on GaAs regardless of the substrate crystal plane.

that the immersion time is a key factor. The longer the immersion time, the larger crystals and more dense growth of them.

Figure S5d–f, Supporting Information, shows SEM results of GaAs substrate immersed in hot water at different temperatures of 50 and 80 °C for 30 min as well as at 100 °C for 120 min. It can be concluded that growth temperature of 80 °C provides larger crystals and higher density of them, as compared to 50 °C where no large crystal is grown. It is noticeable that immersing GaAs in boiling water (100 °C) results in a nonuniform surface with porous nature.

Concerning the growth mechanisms of GaOOH crystals, two hypotheses were considered: 1) dissolving + recrystallization or 2) etching + oxidation. If dissolving of GaAs species and their recrystallization on the surface was the growth mechanism, it could be expected that changing the amount of hot water or stirring water affected the growth. We prepared samples by keeping the amount of hot-water constant during immersion, and we also used a stirrer during the immersion. In these experiments, no obvious change was observed in the formation of structures in SEM characterization (not shown here). Thus we excluded dissolving + recrystallization as a dominating growth mechanism. Therefore, the etching of As from the substrate and formation of GaOOH structures via oxidation of the Ga-rich surface was suggested as a possible growth mechanism.

2.3. Non-Radiative Recombination

In general, the top-to-down methods in manufacturing of semiconductor surfaces often cause the formation of harmful surface defects because the material etching breaks atomic bonds increasing atomic-level roughness and disorder. Therefore, one relevant question is how much the presented black GaAs method increases the amount of point defects. To clarify this, we have measured the PL intensity which is known to decrease if the defect density increases at surface regions. We have measured the samples treated only with H_2O because the hot-water immersion leads to the significant oxide formation at GaAs (Figure 1, 2, S1, Supporting Information). Particularly, the GaAs oxidation is expected to cause surface-defect formation and non-radiative recombination.[41–51] In fact, the common target in the surface or interface passivation has been to minimize the GaAs oxidation.

Figure 5 shows PL and reflectance spectra for the GaAs substrate covered with GaOOH micro- and nanocrystals induced by the mere hot-water immersion. PL results show about 8 times increase in the GaAs band-edge luminescence intensity, as compared to the native-oxide-covered GaAs reference (Figure 5a). Concomitantly, the reflectance of the sample with GaOOH crystals is decreased (also mere H_2O_2 immersion decreases reflectance, as shown in Figure S8, Supporting Information). As mentioned earlier, the reflectance does not however decrease to as low level as for the black GaAs surface (Figure 1) when both the H_2O_2 and H_2O immersions were used. Indeed, the GaOOH-covered surface looks gray visually. Moreover, we have observed an increase in the PL emission centered around 400 nm (Figure 5c), in addition to the increased GaAs band-edge emission (Figure 5a). Such a weak blue emission probably arises from the nano- and microcrystals and their defect levels (e.g., oxygen vacancy–induced levels) in the bandgap.[34–37]

PL intensity can strongly depend on surface properties[52,53] because a long diffusion length of the photogenerated carriers, even hundreds of nanometers, enables part of the carriers to reach defect-rich surfaces although the absorption of photons often occurs in the bulk material far from the surfaces. The second surface-induced factor behind the PL intensity variation is related to changes in the light reflection because the absorption of the laser excitation light increases due to the decreased reflectance. Furthermore, the surface structure might increase the PL intensity via enhanced guiding of the light out from the solid (i.e., due to higher light extraction coefficient). Thus, if the reflectivity decreased by factor of 1.5–2 (Figure 5b), then a total factor increasing the PL intensity was between 2.25 and 4, assuming the same sub-factor in both directions of the light propagation. This is an estimation because reflectance measurement system included an

© 2025 The Author(s). Advanced Photonics Research published by Wiley-VCH GmbH

26999293, 0, Downloaded from https://advanced.onlinelibrary.wiley.com/doi/10.1002/adpr.202400200 by University of Turku, Wiley Online Library on [11/08/2025]. See the Terms and Conditions (https://onlinelibrary.wiley.com/terms-and-conditions) on Wiley Online Library for rules of use; OA articles are governed by the applicable Creative Commons License

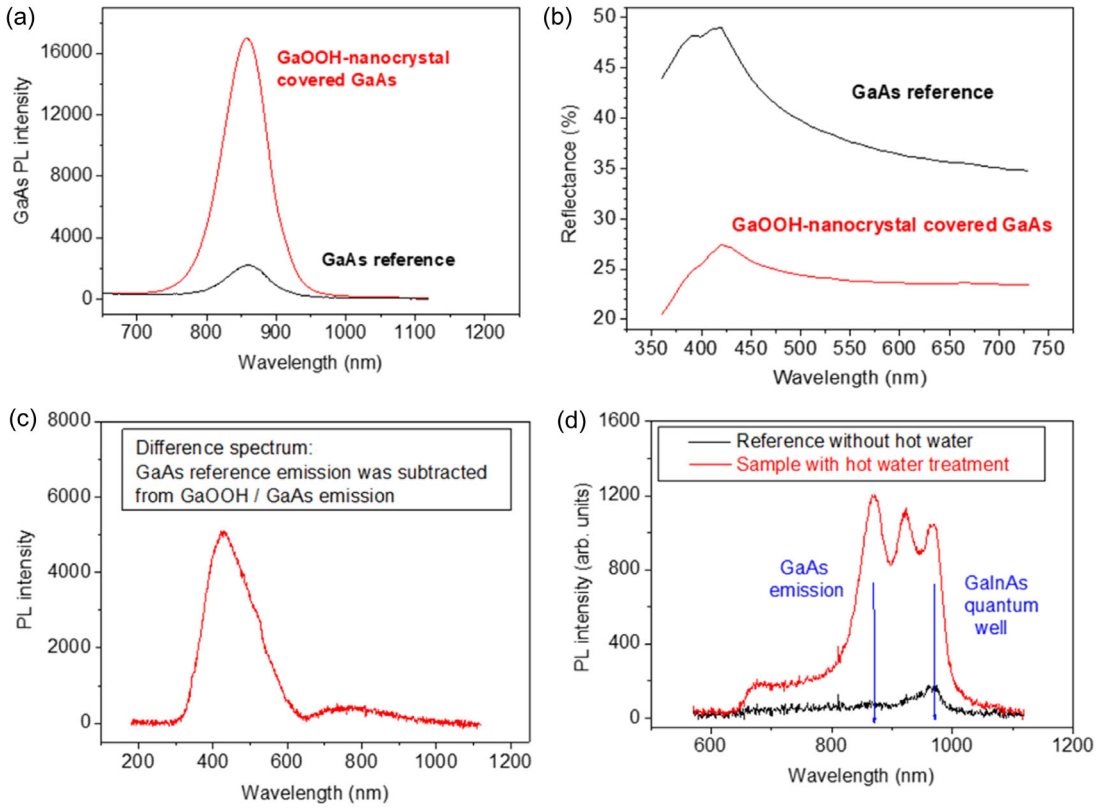

Figure 5. Optical characterization of hot-water-treated GaAs in comparison to a native-oxide-covered GaAs reference. a) Photoluminescence spectra show that the luminescence from GaAs increases due to the presence of nanostructures at the surface. b) Reflectivity of the GaAs surface decreases when the surface contains micro- and nanocrystals. The reflectivity decrease is enhanced at short wavelengths where ultraviolet light (<400 nm) absorption increases. c) GaOOH nanostructures causes a blue emission around 400 nm, which is probably due to defect levels in GaOOH. d) Effects of the hot-water treatment on photoluminescence of GaInAs quantum-well structure capped by GaAs.

integrating sphere, whereas the PL measurement did not. However, it is possible that not all surface oxidations of III–V are harmful to optoelectronic properties.[51]

To clarify the defect issue further, we tested effects of the hot-water treatment on a specific quantum-well (QW) sample, where a GaAs/GaInAs/GaAs heterostructure lies at the surface. Such a near-surface QW emission is very sensitive to the properties of the topmost GaAs layer: the PL intensity from QW decreases significantly when the non-radiative surface recombination increases. However, Figure 5d reveals that the PL intensity from QW increases 6 times approximately due to the hot-water treatment. Thus, the PL results suggest that the black GaAs treatment, where the H_2O immersion is the key oxidation step (Figure 2 and S1, Supporting Information), does not increase non-radiative recombination as compared to the native-oxide-covered GaAs. It is worth noting that the native-oxide-covered surface is not a strict reference sample here because its PL intensity is typically far from that obtained from an optimized heteroepitaxial GaAs interface.[41–51] Furthermore, as discussed earlier, the reduction of PL intensity caused by non-radiative recombination may be masked by the PL enhancement caused by reduced surface reflection. Therefore, future studies in comparison to the high-quality heteroepitaxial GaAs interfaces are needed. Upcoming studies can also elucidate a passivation role of hydrogen atoms incorporated at GaAs surfaces in the H_2O_2 and H_2O immersions.

2.4. Method Integration with Photodetector

Using MSM photodetectors, we have studied a potential route to incorporate the black GaAs method into device processing. MSM photodetectors have gained an increasing interest because of their high speed operation and simple planar structure.[54–61] Here, we used a platinum deposition and lift-off lithography to make fingerlike metal contacts on a semi-insulating GaAs substrate (**Figure 6**a). After that, the black GaAs method was applied, and both the hot H_2O_2 and H_2O immersions were done for the MSM samples that already contained the metal patterns on GaAs.

External quantum efficiency (EQE) of an MSM photodetector describes the number of electron–hole pairs generated by each incident photon,[57,58] using Equation (1):

$$EQE = \frac{hc}{e\lambda} R \tag{1}$$

where h, c, e, λ, and R are the Planck constant, speed of light, elementary charge, wavelength, and responsivity, respectively.

© 2025 The Author(s). Advanced Photonics Research published by Wiley-VCH GmbH

26999293, 0, Downloaded from https://advanced.onlinelibrary.wiley.com/doi/10.1002/adpr.202400200 by University of Turku, Wiley Online Library on [11/08/2025]. See the Terms and Conditions (https://onlinelibrary.wiley.com/terms-and-conditions) on Wiley Online Library for rules of use; OA articles are governed by the applicable Creative Commons License

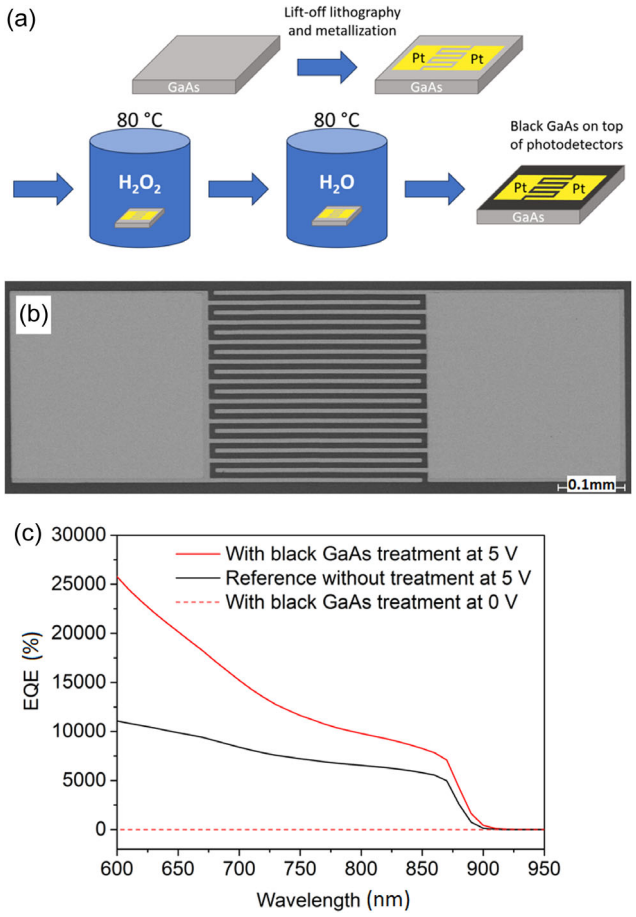

Figure 6. a) Process flow of metal–GaAs–metal photodetector fabrication. b) SEM image of one detector with an interdigital contact geometry after the black GaAs treatment. c) External quantum efficiency (EQE) at a bias of 5 V increased due to black GaAs surface. EQE values at 0 V were similar and near zero for both samples with and without black GaAs treatment.

Responsivity of a photodetector describes the generated current per incident optical power,[57,58] as presented by Equation (2):

$$R = \frac{I_{\text{photo}}}{P_{\text{opt}}} \tag{2}$$

where I_{photo} and P_{opt} are the photocurrent and incident optical power, respectively.

EQE of the fabricated detectors was measured in the wavelength range of 600–950 nm with a 10 nm step. EQE was calculated from measured photocurrent according to Equation (1) and (2). The determined EQE values with 5 V bias are significantly higher than 100% for both the black GaAs–treated and reference samples, which is consistent the previously observed high EQE values for different MSM detectors.[54–60] The exact mechanism behind such high EQE is still unknown, but similar high EQEs have been discussed to arise from an imbalance between the electron and hole drift components in the current transport, due to for example differences between the electron and hole mobilities or trapping of holes in long-lifetime trap levels.[62–65]

Figure 6 shows that EQE has increased for the detectors treated by the black GaAs recipe, which is consistent with the aforementioned findings that the reflectivity at GaAs surfaces has decreased and the PL intensity has increased. Metal contact morphology is not degraded during the black GaAs treatment, as shown by SEM (Figure 6b). Therefore, the results indicate that it is possible to use the black GaAs method after making the metal contacts, providing a potential integration path with device processes. Future studies can clarify what kind of effects the H_2O_2 and H_2O immersions have on metal–GaAs interface structures.

3. Conclusion

The antireflective black GaAs surface was found to form in a surprisingly facile way by keeping GaAs crystals first in the hot H_2O_2 solution and then in the hot H_2O solution. A proper combination of these two immersions decreased the diffused reflectivity to 1/10 of the native GaAs surface reference and the specular reflectivity even below 1% in a broad wavelength range. The measurements of structural and chemical properties showed that the H_2O_2 immersion step caused a porous GaAs surface while the H_2O immersion step increased the nanocrystal growth. The mere hot-water treatment of GaAs was found to induce the growth of GaOOH nano- and microcrystals at GaAs. We suggested that the GaOOH nanocrystal formation in the hot water was induced by the preferential etching of As and oxidation of the Ga-enriched surface. The PL measurements suggested that the hot-water immersion did not increase the surface non-radiative recombination, as compared to the native-oxide-covered GaAs reference. However, this issue still remained open because a reduced surface reflectivity affected the PL intensities, and due to the lack of high-quality PL reference samples. Finally, MSM photodetectors were used as a test platform to integrate the black GaAs method with device processing. Making the H_2O_2 and H_2O immersions for the detector sample, which contained already the metal-contact patterns, increased the EQE of the MSM components.

4. Experimental Section

GaAs crystals were cut from the following 2-inch wafers: n-GaAs(111)A and n-GaAs(111)B, and n-GaAs(100) and *p*-GaAs(100). The samples were pre-cleaned in isopropanol (IPA) in an ultrasonic bath and then they were inserted into a solution of HCl:IPA (1:3) for three minutes followed by IPA immersion for 1 min. To investigate the effect of the pre-cleaning method, some samples were treated with different chemicals: NH_4OH:H_2O (1:3) and H_2SO_4:H_2O (1:10). After the pre-cleaning step, samples were inserted into a beaker of hot hydrogen peroxide followed by hot deionized water (resistivity of 21 MΩcm) on top of a hot plate. The water temperature was set and kept constant at 80 °C for GaAs samples. The immersion time was varied between 5 and 240 min.

A separate QW sample was grown by molecular beam epitaxy. This epitaxial III–V heterostructure contained the following layers from the top to the bottom: GaInP (100 nm)/GaAs (100 nm)/GaInAs (6 nm)/GaAs (100 nm)/GaInP (400 nm)/GaAs (100 nm)/n-GaAs substrate. The grown wafer was cut into pieces. Before treatments, the top-most GaInP layer was selectively removed by HCl etching.

SEM imaging was performed by Thermo Scientific Apreo S field-emission SEM equipped with Oxford Instruments Ultim Max 100 EDX detector. The secondary and backscattered electron images were observed

© 2025 The Author(s). Advanced Photonics Research published by Wiley-VCH GmbH

26999293, 0, Downloaded from https://advanced.onlinelibrary.wiley.com/doi/10.1002/adpr.202400200 by University of Turku, Wiley Online Library on [11/08/2025]. See the Terms and Conditions (https://onlinelibrary.wiley.com/terms-and-conditions) on Wiley Online Library for rules of use; OA articles are governed by the applicable Creative Commons License

in high vacuum using Everhart–Thornley and in-lens/in-column Trinity detectors. No coating of the samples was done prior to the imaging.

PL was measured together with a reference sample without any structures. PL measurements were done utilizing a (LOTIS TII Nd:YAG) neodymium-doped yttrium aluminum garnet laser system LS-2134UTF using the 266 or 532 nm line, and the spectra were recorded with an AvaSpec HS-TEC spectrometer. Line pass filters Newport 10LF10-266 and Thorlabs FLH532 were used, and integration time was 3 and 1 s with 266 and 532 nm, respectively.

Reflectance was measured by two different instruments. The spectrum in Figure 1a was the specular reflection, measured perpendicular to the surface with Accent RPM2000 PL instrument. A highly reflective mirror was used as a control sample. The reflectance of this reference was expected to be ideal, 100%, meaning that the real reflectance of the black GaAs might be slightly smaller than that shown in Figure 1a. In contrast, the reflectance curves in Figure 1b were measured with a Konica Minolta CM-2300d handheld spectrometer using D65 illuminant and 10° observer with operational wavelength range of 360−740 nm. An integrating sphere housing a diffuse inner lining was used to measure a diffused or Lambertian type reflection. This instrument was calibrated with measuring a white reference disk Konica Minolta CM-A145 for maximum reflectance and empty room from at least 1 meter away from any surfaces and/or lights in a dark room for the minimum reflectance level, i.e., dark reference. The target mask was selected so that there would be no interferences to the measurement result from other materials except the sample.

Crystalline structures were measured utilizing both laboratory X-ray diffraction (XRD) and Synchroton XRD. The laboratory XRD measurements were performed using an Empyrean X-ray diffractometer with five axis goniometer and proportional counter detector and with X-ray radiation containing the components of Cu $K\alpha_1$ and $K\alpha_2$. The 2θ measurements were done between $2\theta = 15°$ and $2\theta = 65°$. The incident diffraction angle was set to 1°. Synchrotron measurements were performed at room temperature using a six circle diffractometer (Huber 5020) with MYTHEN detector (Dectris) at the angle-dispersive XRD beamline (BL-12) at Indus-2 Synchrotron source, RRCAT, India.[66] The data were collected at 14.670 keV and at 0.3°, 0.6°, 1.0°. incidence angles. The energy/wavelength was calibrated using XRD pattern of standard Si (National Institute of Standards and Technology). Patterns were analyzed with available international centre for diffraction data (ICDD)-XRD database of GaAs, Ga_2O_3 (rhombohedral R and monoclinic M), $Ga(OH)_3$ (cubic C and tetragonal T), and GaOOH (orthorhombic O but different unit cell size).

XPS was utilized to measure chemical composition of the surfaces. XPS was done with Thermo Scientific Nexsa system equipped with monochromatized Al Kα radiation source, dual-mode charge compensation, and MAGCIS source for monoatomic and cluster etching and depth profiling. The wide energy range survey spectra and high-resolution core-level spectra were collected with pass energies of 200 and 50 eV, respectively. The X-ray spot size was 200 µm.

STEM images and EDX maps were acquired by FEI Titan Themis 200 microscope, equipped with Bruker/FEI SuperX EDX system at 200 kV. The thin cross-sectional sample for STEM studies was prepared by focused ion beam using the in situ lift-out technique in FEI Helios NanoLab 600 SEM-(FIB) focused ion beam system. To protect the surface of the sample from milling by the ion beam during thin sample preparation, the area of interest was covered by a protection layer, consisting of a thin carbon layer deposited via electron beam–assisted deposition and a 1 µm thick platinum layer deposited via ion beam–assisted deposition at low ion beam current.

MSM detectors were fabricated on semi-insulating GaAs wafer pieces using platinum as a metal contact. The contacts were defined with lift-off lithography using AZ ECI 3012 photoresist, AZ 726 MIF developer and acetone as stripper. Contact patterning was done by direct laser writing with Kloé Dilase 250 laser writer. Platinum was deposited by sputtering. Photoelectrical characterization setup consisted of a 90 W tungsten lamp, monochromator, optical chopper connected to a lock-in amplifier and electrical measurement circuit. Light was focused to the detector active area with an objective, and light spot area was smaller than detector active area. Optical power was calibrated by a Si photodiode.

The EQE measurements were measured using a self-made system containing a 250 W quartz tungsten halogen lamp (Thermo Oriel) run at 90 W power, a ¼ m Digikröm monochromator (CVI), a *P*-9202-4 photocurrent/voltage amplifier (Gigahertz-Optik), SR450 chopper (Stanford Research Systems), a 15x, 0.28 NA long working distance mirror objective (Edmund optics), SR830 DSP lock-in amplifier (Stanford Research Systems), and a LabVIEW-based software for data acquisition. (NIST)-traceable national institute of standards and technology calibrated Si photodiode (FDS100-CAL, from Thorlabs Inc.) was used as a reference detector. In the EQE measurement system, the sample and the reference detector were measured separately, i.e., one after another.

Supporting Information

Supporting Information is available from the Wiley Online Library or from the author.

Acknowledgements

This work has been supported by the University of Turku Graduate School (UTUGS), the Academy of Finland (via the project #296469), Business Finland (via the project RONASEC), and Wihuri Foundation (Z.J.R.). The XPS and SEM/EDX experiments were carried out using resources provided by Materials Research Infrastructure (MARI). Wihuri Foundation is also acknowledged for supporting UTU clean room facilities.

Open access publishing facilitated by Turun yliopisto, as part of the Wiley - FinELib agreement.

Conflict of Interest

Part of authors at University of Turku has submitted a patent application about results.

Data Availability Statement

The data that support the findings of this study are available from the corresponding author upon reasonable request.

Keywords

antireflection coatings, black GaAs, photodetectors, wet chemical methods

Received: November 26, 2024
Revised: April 24, 2025
Published online:

[1] S. Koynov, M. S. Brandt, M. Stutzmann, *Appl. Phys. Lett.* **2006**, *88*, 203107.
[2] Y.-L. Chueh, Z. Fan, K. Takei, H. Ko, R. Kapadia, A. A. Rathore, N. Miller, K. Yu, M. Wu, E. E. Haller, A. Javey, *Nano Lett.* **2010**, *10*, 520.
[3] M. De Jarld, J. C. Shin, W. Chern, D. Chanda, K. Balasundaram, J. A. Rogers, X. Li, *Nano Lett.* **2011**, *11*, 5259.
[4] L.-K. Yeh, K.-Y. Lai, G.-J. Lin, P.-H. Fu, H.-C. Chang, C.-A. Lin, J.-H. He, *Adv. Energy Mat.* **2011**, *1*, 506.
[5] J. Oh, H. C. Yuan, H. M. Branz, *Nat. Nanotechn.* **2012**, *7*, 743.
[6] S. Ravipati, J. Shieh, F.-H. Ko, C.-C. Yu, H.-L. Chen, C.-T. Wu, S.-H. Chen, *Energy Environ. Sci.* **2012**, *5*, 7601.

© 2025 The Author(s). Advanced Photonics Research published by Wiley-VCH GmbH

26999293, 0, Downloaded from https://advanced.onlinelibrary.wiley.com/doi/10.1002/adpr.202400200 by University of Turku, Wiley Online Library on [11/08/2025]. See the Terms and Conditions (https://onlinelibrary.wiley.com/terms-and-conditions) on Wiley Online Library for rules of use; OA articles are governed by the applicable Creative Commons License

[7] J. Tommila, A. Aho, A. Tukiainen, V. Polojärvi, J. Salmi, T. Niemi, M. Guina, *Progr. Photovoltaics* **2013**, *21*, 1158.
[8] D. Liang, Y. Kang, Y. Huo, Y. Chen, Y. Cui, J. S. Harris, *Nano Lett.* **2013**, *13*, 4850.
[9] X. Liu, P. R. Coxon, M. Peters, B. Hoex, J. M. Cole, D. J. Fray, *Energy Environ. Sci.* **2014**, *7*, 3223.
[10] P. Lova, V. Robbiano, F. Cacialli, D. Comoretto, C. Soci, *ACS Appl. Mat. Int.* **2018**, *10*, 33434.
[11] C. Huo, J. Wang, H. Fu, X. Li, Y. Yang, H. Wang, A. Mateen, G. Farid, K.-Q. Peng, *Adv. Funct. Mat.* **2020**, *30*, 2005744.
[12] S. Namiki, H.-C. Huang, J. Soares, X. Wu, J. D. Kim, B. Jiang, V. Srikumar, X. Li, *Adv. Photonics Res.* **2021**, *2*, 2000134.
[13] Y. Cheng, L. Ding, *SusMat* **2021**, *1*, 324.
[14] P. Mc Kearney, S. Schäfer, X. Liu, S. Paulus, I. Lebershausen, B. Radfar, V. Vähänissi, H. Savin, S. Kontermann, *Adv. Photonics Res.* **2024**, *5*, 2300281.
[15] H. Park, T. Mariyappan, H. D. Nguyen, R. C. Dang, M. Kim, *Adv. Mat. Technol.* **2024**, *9*, 2400062.
[16] Y. Qiu, L.-F. Ren, L. Xia, J. Shao, Y. Zhao, B. Van der Bruggen, *Chem. Eng. J.* **2022**, *438*, 135562.
[17] M. Ruberti, *Sci. Total Environ.* **2023**, *858*, 159873.
[18] E. Gallagher, P. Bezard, L. Boakes, A. Firrincieli, C. Rolin, L. Ragnarsson, Sustainable semiconductor manufacturing: lessons for lithography and etch, *Proceedings Advanced Etch Technology and Process Integration for Nanopatterning XII*, **2023**, 12499 124990F.
[19] G. F. Brescia, Sustainability in the Semiconductor Industry, Power Electr. News **2024**, April 26.
[20] M. B. Panish, I. Hayashi, S. Sumski, *Appl. Phys. Lett.* **1970**, *16*, 326.
[21] R. D. Dupuis, P. D. Dapkus, N. Jr. Holonyak, E. A. Rezek, R. Chin, *Appl. Phys. Lett.* **1978**, *32*, 295.
[22] D. M. Kuchta, A. V. Rylyakov, F. E. Doany, C. L. Schow, J. E. Proesel, C. W. Baks, P. Westbergh, J. S. Gustavsson, A. Larsson, *IEEE Phot. Techn. Lett.* **2015**, *27*, 577.
[23] Z. Xie, Z. Zhou, L. Li, Z. Deng, H. Ji, B. Chen, *IEEE J. Select. Top. Quant. Electr.* **2022**, *28*, 3801007.
[24] J. Li, C. Jiang, H. Liu, Y. Zhang, H. Zhai, X. Wei, Q. Wang, G. Wu, C. Li, X. Ren, *Adv. Photonics Res.* **2024**, *5*, 2300348.
[25] J. J. Schermer, P. Mulder, G. J. Bauhuis, P. K. Larsen, G. Oomen, E. Bongers, *Prog. Photovolt: Res. Appl.* **2005**, *13*, 587.
[26] F.-L. Chen, A. Cattoni, R. D. Lépinau, A. W. Walker, O. Höhn, D. Lackner, G. Siefer, M. Faustini, N. Vandamme, J. Goffard, B. Behaghel, C. Dupuis, N. Bardou, F. Dimroth, S. Collin, , *Nat. Energy* **2019**, *4*, 761.
[27] I. Mathews, D. Quinn, J. Justice, A. Gocalinska, E. Pelucchi, R. Loi, J. O'Callaghan, B. Corbett, *Adv. Mater. Technol.* **2020**, *5*, 2000048.
[28] N. Hong, D.-M. Geum, T. S. Kim, S. Ahn, J.-H. Han, D. Jung, G. Ryu, S. Kim, K. J. Yu, W. J. Choi, *Adv. Photonics Res.* **2021**, *2*, 2000051
[29] Y. Yun, S. Moon, S. Kim, J. Lee, *Solar Energy Mat. Sol. Cells* **2022**, *246*, 111930.
[30] M. N. Beattie, H. Helmers, G. P. Forcade, C. E. Valdivia, O. Höhn, K. Hinzer, *IEEE J. Photovolt.* **2023**, *13*, 113.
[31] A. Zumeit, A. S. Dahiya, A. Christou, R. Mukherjee, R. Dahiya, *Adv. Mat. Technol.* **2022**, *7*, 2200772.
[32] Y. Xu, R. Ahmed, J. Zheng, E. R. Hoglund, Q. Lin, E. Berretti, A. Lavacchi, G. Zangari, *Small* **2020**, *16*, 2003112.
[33] S. Cao, Z. Kang, Y. Yu, J. Du, L. German, J. Li, X. Yan, X. Wang, Y. Zhang, *Adv. Energy Mat.* **2020**, *10*, 1902985.
[34] C. H. Liang, G. W. Meng, G. Z. Wang, Y. W. Wang, L. D. Zhang, S. Y. Zhang, *Appl. Phys. Lett.* **2001**, *78*, 3202.
[35] K.-W. Chang, J.-J. Wu, *Adv. Mat.* **2004**, *16*, 545.
[36] Y. Zhao, R. L. Frost, J. Yang, W. N. Martens, *J. Phys. Chem. C* **2008**, *112*, 3568.
[37] M. Muruganandham, R. Amutha, M. S. M. A. Wahed, B. Ahmmad, Y. Kuroda, R. P. S. Suri, J. J. Wu, M. E. T. Sillanpää, *J. Phys. Chem. C* **2012**, *116*, 44.
[38] P. Pedram, A. Zavabeti, N. Syed, A. Slassi, C. K. Nguyen, B. Fornacciari, A. Lamirand, J. Galipaud, A. Calzolari, R. Orobtchouk, A. Boes, T. Daeneke, S. Cueff, A. Mitchell, C. Monat, *Adv. Photonics Res.* **2024**, *5*, 2300252.
[39] S. J. Pearton, J. Yang, P. H. Cary, F. Ren, J. Kim, M. J. Tadjer, M. A. Mastro, *Appl. Phys. Rev.* **2018**, *5*, 011301.
[40] Z. Muhammad, Y. Wang, Y. Zhang, P. Vallobra, S. Peng, S. Yu, Z. Lv, H. Cheng, W. Zhao, *Adv. Mat. Technol.* **2023**, *8*, 2200539.
[41] W. Wilmsen, *Physics And Chemistry Of III-V Compound Semiconductor Interfaces*, Springer, Plenum **1985**.
[42] E. Yablonovitch, C. J. Sandroff, R. Bhat, T. Gmitter, *Appl. Phys. Lett.* **1987**, *51*, 439.
[43] M. Passlack, J. K. Abrokwah, R. Droopad, Z. Yu, C. Overgaard, S. I. Yi, M. Hale, J. Sexton, A. C. Kummel, *IEEE Electr. Dev. Lett.* **2002**, *23*, 508.
[44] C. L. Hinkle, A. M. Sonnet, E. M. Vogel, S. McDonnell, G. J. Hughes, M. Milojevic, B. Lee, F. S. Aguirre-Tostado, K. J. Choi, J. Kim, R. M. Wallace, *Appl. Phys. Lett.* **2007**, *91*, 163512.
[45] P. D. Ye, *J. Vac. Sci. Technol. A* **2008**, *26*, 697.
[46] H. Hasegawa, M. Akazawa, *Appl. Surf. Sci.* **2008**, *254*, 8005.
[47] *Fundamentals Of III-V Semiconductor MOSFETs*, edited by S. Oktyabrsky and P. D. Ye, Springer **2010**.
[48] Y.-C. Byun, S. Choi, Y. An, P. C. McIntyre, H. Kim, *ACS Appl. Mat. Int.* **2015**, *7*, 7445.
[49] Z. Li, H. H. Tan, C. Jagadish, L. Fu, *Adv. Mater. Technol.* **2018**, *3*, 1800005.
[50] M. Hong, H. W. Wan, K. Y. Lin, Y. C. Chang, M. H. Chen, Y. H. Lin, T. D. Lin, T. W. Pi, J. Kwo, *Appl. Phys. Lett.* **2017**, *111*, 123502.
[51] P. Laukkanen, M. P. J. Punkkinen, M. Kuzmin, K. Kokko, J. Lång, R. M. Wallace, *Appl. Phys. Rev.* **2021**, *8*, 011309.
[52] T. Saitoh, H. Iwadate, H. Hasegawa, *Jpn. J. Appl. Phys.* **1991**, *30*, 12B.
[53] M. Passlack, M. Hong, E. F. Schubert, J. R. Kwo, J. P. Mannaerts, S. N. G. Chu, N. Moriya, F. A. Thiel, *Appl. Phys. Lett.* **1995**, *66*, 625.
[54] C.-T. Lee, H.-Y. Lee, *IEEE Phot. Techn. Lett.* **2005**, *17*, 462.
[55] F. Zhuge, Z. Zheng, P. Luo, L. Lv, Y. Huang, H. Li, T. Zhai, *Adv. Mat. Technol.* **2017**, *2*, 1700005.
[56] G. Chen, J. Goyvaerts, S. Kumari, J. Van Kerrebrouck, M. Muneeb, S. Uvin, Y. Yu, G. Roelkens, *Opt. Expr.* **2018**, *26*, 6351.
[57] L. Shi, K. Chen, A. Zhai, G. Li, M. Fan, Y. Hao, F. Zhu, H. Zhang, Y. Cui, *Las. Photonics Rev.* **2021**, *15*, 2000401.
[58] Z. Li, Z. He, C. Xi, F. Zhang, L. Huang, Y. Yu, H. H. Tan, C. Jagadish, L. Fu, *Adv. Mat. Technol.* **2023**, *8*, 2202126.
[59] S. Huang, G. Deng, X. Jin, Y. Lu, G. Song, H. Huang, P. Zhao, C. Zhang, J. Yao, Q. Wu, J. Xu, *Optic. Mat.* **2020**, *110*, 110474.
[60] J. Khan, R. T. M. Ahmad, J. Tan, R. Zhang, U. Khan, B. Liu, *SmartMat* **2023**, *4*, e1156.
[61] D. Wei, B. Guo, A. A. Dadey, J. A. McArthur, J. Bai, S. R. Bank, J. C. Campbell, *Adv. Photonics Res.* **2024**, *5*, 2400090
[62] S. F. Soares, *Jpn. J. Appl. Phys.* **1992**, *31*, 210.
[63] M. Klingenstein, J. Kuhl, J. Rosenzweig, C. Moglestue, A. Hulsmann, J. Schneider, K. Köhler, *Solid State Electron* **1994**, *37*, 333.
[64] O. Katz, V. Garber, B. Meyler, G. Bahir, J. Salzman, *Appl. Phys. Lett.* **2001**, *79*, 1417.
[65] S. Rathkanthiwar, A. Kalra, S. V. Solanke, N. Mohta, R. Muralidharan, S. Raghavan, D. N. Nath, *J. Appl. Phys.* **2017**, *121*, 164502.
[66] A. K. Sinha, A. Sagdeo, P. Gupta, A. Upadhyay, A. Kumar, M. N. Singh, R. K. Gupta, S. R. Kane, A. Verma, S. K. Deb, *J. Phys. Conf.* **2013**, *425*, 072017.

© 2025 The Author(s). Advanced Photonics Research published by Wiley-VCH GmbH

26999293, 0, Downloaded from https://advanced.onlinelibrary.wiley.com/doi/10.1002/adpr.202400200 by University of Turku, Wiley Online Library on [11/08/2025]. See the Terms and Conditions (https://onlinelibrary.wiley.com/terms-and-conditions) on Wiley Online Library for rules of use; OA articles are governed by the applicable Creative Commons License